JACS
JOURNAL OF THE AMERICAN CHEMICAL SOCIETY
pubs.acs.org/JACS
Article

High-Temperature Pulse Method for Nanoparticle Redispersion

Hua Xie,[#] Min Hong,[#] Emily M. Hitz, Xizheng Wang, Mingjin Cui, Dylan J. Kline, Michael R. Zachariah, and Liangbing Hu*

Cite This: J. Am. Chem. Soc. 2020, 142, 17364−17371
Read Online
ACCESS | Metrics & More | Article Recommendations | Supporting Information

ABSTRACT: Nanoparticles suffer from aggregation and poisoning issues (e.g., oxidation) that severely hinder their long-term applications. However, current redispersion approaches, such as continuous heating in oxidizing and reducing environments, face challenges including grain growth effects induced by long heating times as well as complex procedures. Herein, we report a facile and efficient redispersion process that enables us to directly transform large aggregated particles into nanoscale materials. In this method, a piece of carbon nanofiber film was used as a heater and high treatment temperature (~1500−2000 K) is rapidly elevated and maintained for a very short period of time (100 ms), followed by fast quenching back to room temperature at a cooling rate of 10^5 K/s to inhibit sintering. With these conditions we demonstrate the redispersion of large aggregated metal oxide particles into metallic nanoparticles just ~10 nm in size, uniformly distributed on the substrate. Furthermore, the metallic states of the nanoparticles are renewed during the heat treatment through reduction. The redispersion process removes impurities and poisoning elements, yet is able to maintain the integrity of the substrate because of the ultrashort heating pulse time. This method is also significantly faster (ca. milliseconds) compared to conventional redispersion treatments (ca. hours), providing a pragmatic strategy to redisperse degraded particles for a variety of applications.

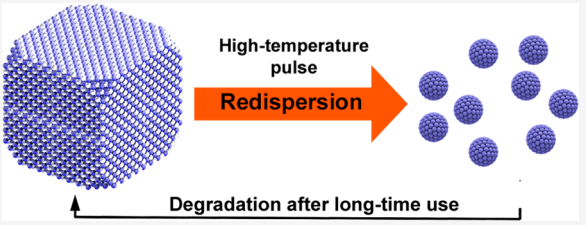

INTRODUCTION

Nanoparticles, although widely employed in various domains such as batteries and catalysis,[1−5] face severe degradation issues after long operation times.[6,7] Such degradation generally stems from the morphology changes of nanoparticles as they aggregate and coalesce into larger particles, which can compromise performance.[8−10] Although smaller nanoparticles do not always possess high catalytic performance,[11−13] an average particle size of ~10 nm or less is necessary to guarantee sufficient active sites. Additionally, some metal nanoparticles gradually become oxidized or chlorinated during long-term operation.[14−17] These poisonous impurities are frequently adsorbed on active sites and block routes.[18−21]

Redispersing agglomerated particles generally requires heat treatment in a first oxidative and then reducing atmosphere, which is typically conducted at heating rates of a maximum of 10 °C/min to a thermostatic plateau at 600−1000 K. After treatment, the samples are slowly cooled down to room temperature, and this process is generally cycled to achieve an observable decrease in particle size,[22] thus lengthening the processing time. Additionally, redispersion highly depends on the dimensions of the coalesced particles, with larger materials taking even longer.[23,24] Particles possess better migration capability at higher temperature;[25] however, sintering will inevitably occur at such temperatures under prolonged treatment, particularly in reducing environments.[26] As a result, conventional redispersion techniques with continuous and excessive heat input neutralize the effectiveness of redispersion. Additionally, reported redispersion approaches have generally focused on noble-metal particles, which regain their metallic states more easily. Nonprecious transition metals, which undergo more severe aggregation and oxidation issues, are more difficult to address.[27] Finally, these approaches are not practical for nanoparticles supported by carbon-based materials (a common catalytic platform),[6] as carbon substrates cannot be stable under high-temperature oxidative environments.

RESULTS AND DISCUSSION

To overcome these challenges, we have designed a novel high-temperature pulse-based approach to redispersion in which a piece of carbon nanofiber film (CNF) was used as a heater. We rapidly elevate the heating temperature up to 2000 K while shortening the treatment duration time to just ~100 ms, followed by quenching to room temperature at a fast cooling rate of 10^5 K/s. In this manner, we were able to convert nanoparticles that had become aggregated (several hundred nanometers to tens of micrometers in size) after catalytic use back into nanoscale particles that continued to retain their

Received: May 10, 2020
Published: September 11, 2020

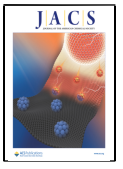

https://dx.doi.org/10.1021/jacs.0c04887
J. Am. Chem. Soc. 2020, 142, 17364−17371

good dispersion after treatment (Figure 1a). The high temperature enables the fast mobility of the metal atoms for improved dispersion, while the heating and quenching durations are short enough to inhibit the occurrence of particle growth. Figure 1b presents the comparison of platinum nanoparticles before and after redispersion, which present a uniform distribution after the high-temperature pulse treatment and the oxygen reduction performance after the redispersion presents pronounced improvement (Figure S1, Supporting Information). This high-temperature pulse approach applies not only to noble metals but also to nonprecious transition metals. This approach can be applied to various substrates, including carbon, making it widely applicable for redispersing various catalytic materials.

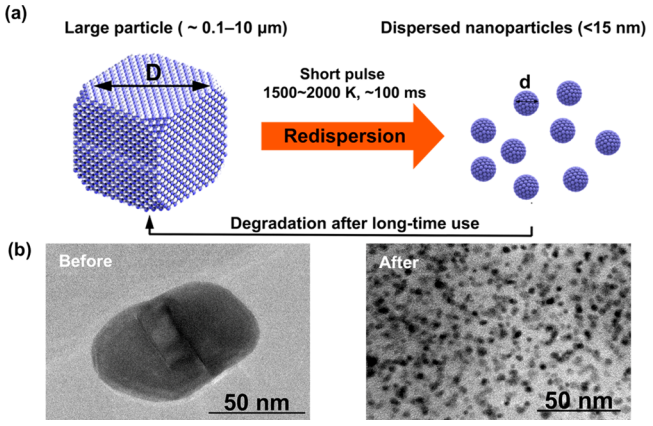

Figure 1. (a) Schematic demonstrating the high-temperature pulse method for nanoparticle redispersion. A controlled current pulse was applied to instantaneously generate a high-temperature environment, dispersing aggregated particles to nanoscale components. (b) Transmission electron microscopy (TEM) images of the morphology of Pt nanoparticles before and after the high-temperature pulse treatment.

To demonstrate this pulse redispersion technique, as proof-of-concept we investigated copper nanoparticles since they are promising as catalysts for various reactions in the petrochemical industry.[28−31] We employed an amorphous CNF film as the nanoparticle redispersion microheater (see Methods for details). The CNF film was carbonized at a low temperature (580 °C) to maintain a high resistivity. Its resistance was carefully tuned by controlling its dimensions to enable the generation of high temperature via Joule heating, which helps redipserse and reduce the aggregated nanoparticles. The CNF film also functioned as the carbon substrate for the particle redispersion. We applied a controlled transient current to the CNF film for ∼100 ms to instantaneously elevate the local temperature to ∼1800 K in an argon atmosphere. The temperature was measured by imaging the light emitted from the Joule-heated CNF film using a high-speed spectrometer camera and fitting the spectrum with an adjusted blackbody radiation relation. After the high-temperature pulse, the substrate rapidly cools to ambient temperature at a rate of 10^5 K/s.

Figure 2a shows a scanning electron microscopy (SEM) image of the large copper oxide (CuO) particles (2−20 μm in size) that we premixed with carbon nanofibers (CNFs) via sonication. Figure 2b shows a transmission electron microscopy (TEM) image of the resulting nanoparticles on the CNF substrate after the high-temperature pulse redispersion, which causes a reduction in the average particle size down to 11 nm. The inset of Figure 2b presents the electron diffraction pattern of the Cu nanoparticles, in which two polycrystalline diffraction rings indicate the (111) and (200) planes of the nanocrystals, respectively, verifying the crystallinity of the redispersed Cu nanoparticles. The X-ray diffraction (XRD)

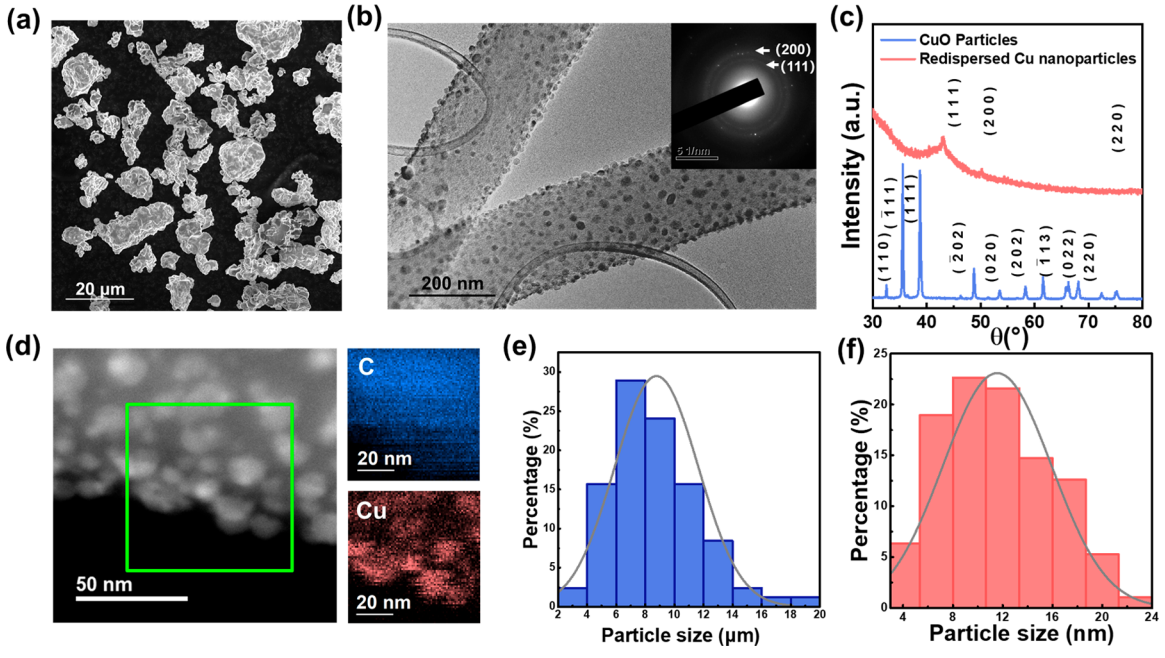

Figure 2. Characterization of Cu nanoparticle redispersion on a CNF substrate after the high-temperature pulse. (a) SEM image of the large CuO particles. (b) TEM image of the redispersed Cu nanoparticles anchored on the CNF substrate. The inset image demonstrates the electron diffraction rings of the Cu nanoparticles. (c) XRD pattern of the Cu nanoparticles confirms the reduced metal after regeneration. (d) EDX mapping of the Cu nanoparticles on the CNF substrate. (e, f) Particle size distribution of the CuO particles (e) before and (f) after redispersion.

https://dx.doi.org/10.1021/jacs.0c04887
J. Am. Chem. Soc. 2020, 142, 17364−17371

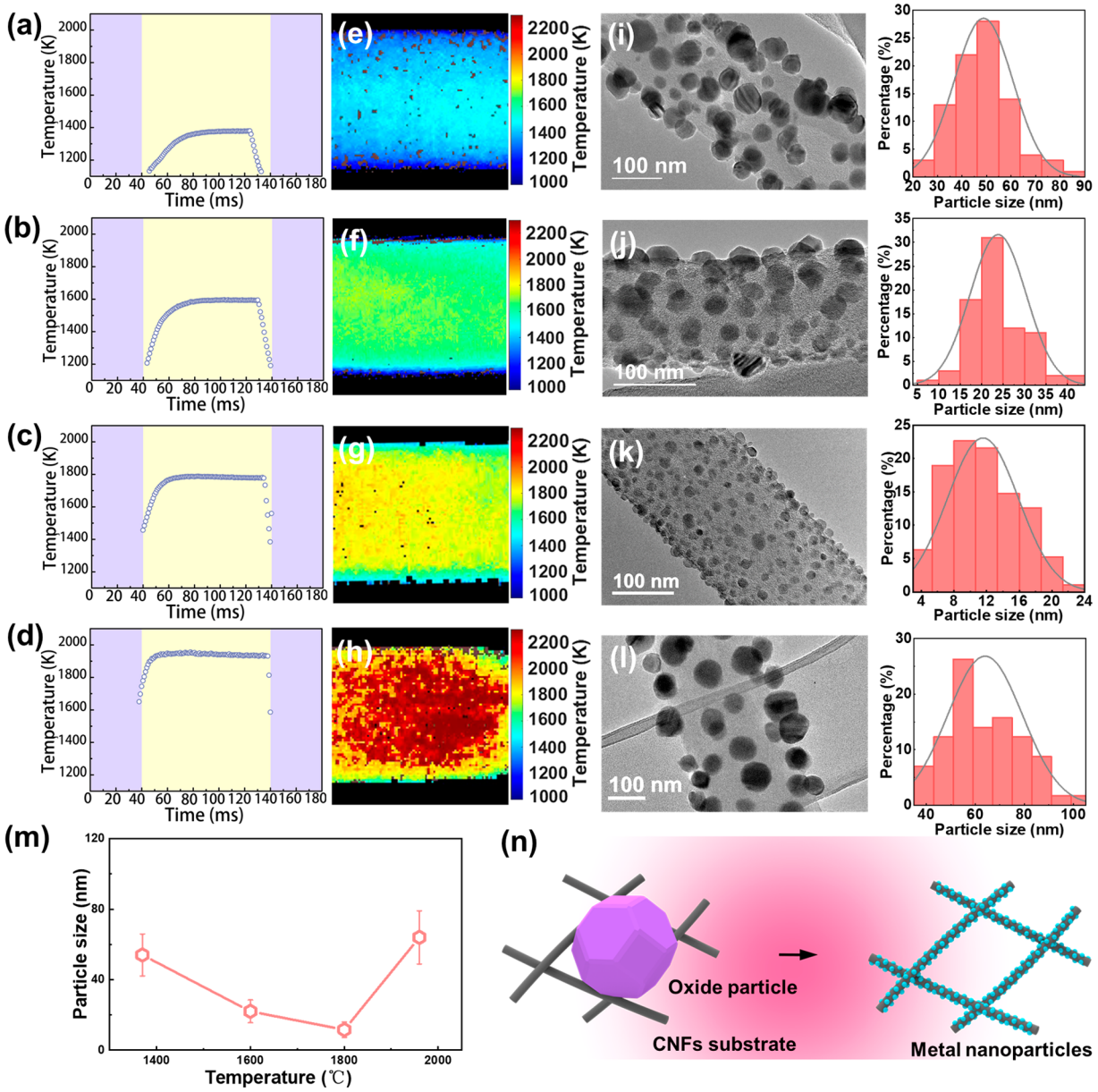

Figure 3. Temperature dependence of the particle size distribution. (a)−(d) The transient temperature profiles of the CNF films, which reach high-temperature plateaux of 1380, 1600, 1800, and 1950 K, respectively. The heating duration was maintained for each sample at 100 ms. (e)−(h) Temperature distribution mapping of the CNF films during each high-temperature hold. (i)−(l) TEM images of the redispersed Cu nanoparticles and their size distribution at the different temperatures. (m) Relationship between the average particle size and temperature. The average particle size decreases with temperature up until 1800 K, at which point the average particle size begins to increase. (n) Schematic to illustrate the transient redispersion process.

patterns of the particles before and after the high-temperature pulse treatment are presented in Figure 2c, confirming the successful reduction of CuO to Cu nanoparticles in the redispersion process. The XRD results show that the diffraction peaks at 43.2° and 50.3° correspond to (111) and (200) planes, which corroborate the electron-diffraction observations in TEM. Scanning transmission electron microscopy (STEM) images and energy-dispersive X-ray spectroscopic (EDS) mapping in Figure 2d further illustrate the uniform distribution of Cu nanoparticles on the carbon substrate. The statistical distribution of the particle diameters before and after the high-temperature pulse treatment, both of which exhibit typical Gaussian shape, are illustrated in Figure 2e,f. The average diameter of the nanoparticles after redispersion was reduced from 8.7 ± 2.9 μm to 11.6 ± 4.3 nm. Inductively coupled plasma mass spectrometry (ICP-MS) was carried out to evaluate the Cu element retention, the result of which showed that the Cu ratios before and after redispersion were 17.3% and 14.2%, respectively, which demonstrates that 82% of the Cu loading was retained. We observed no obvious change in the Raman spectra of the CNF substrate as a result of the 100 ms high-temperature pulse, indicating the good stability of the substrate during treatment (Figure S2). Our approach creates a transient high temperature in a short time, which helps the amorphous carbon to react and reduce the CuO to Cu nanoparticles. Before the occurrence of particle reagglomeration, the sample is already quenched to room temperature.

https://dx.doi.org/10.1021/jacs.0c04887
J. Am. Chem. Soc. 2020, 142, 17364−17371

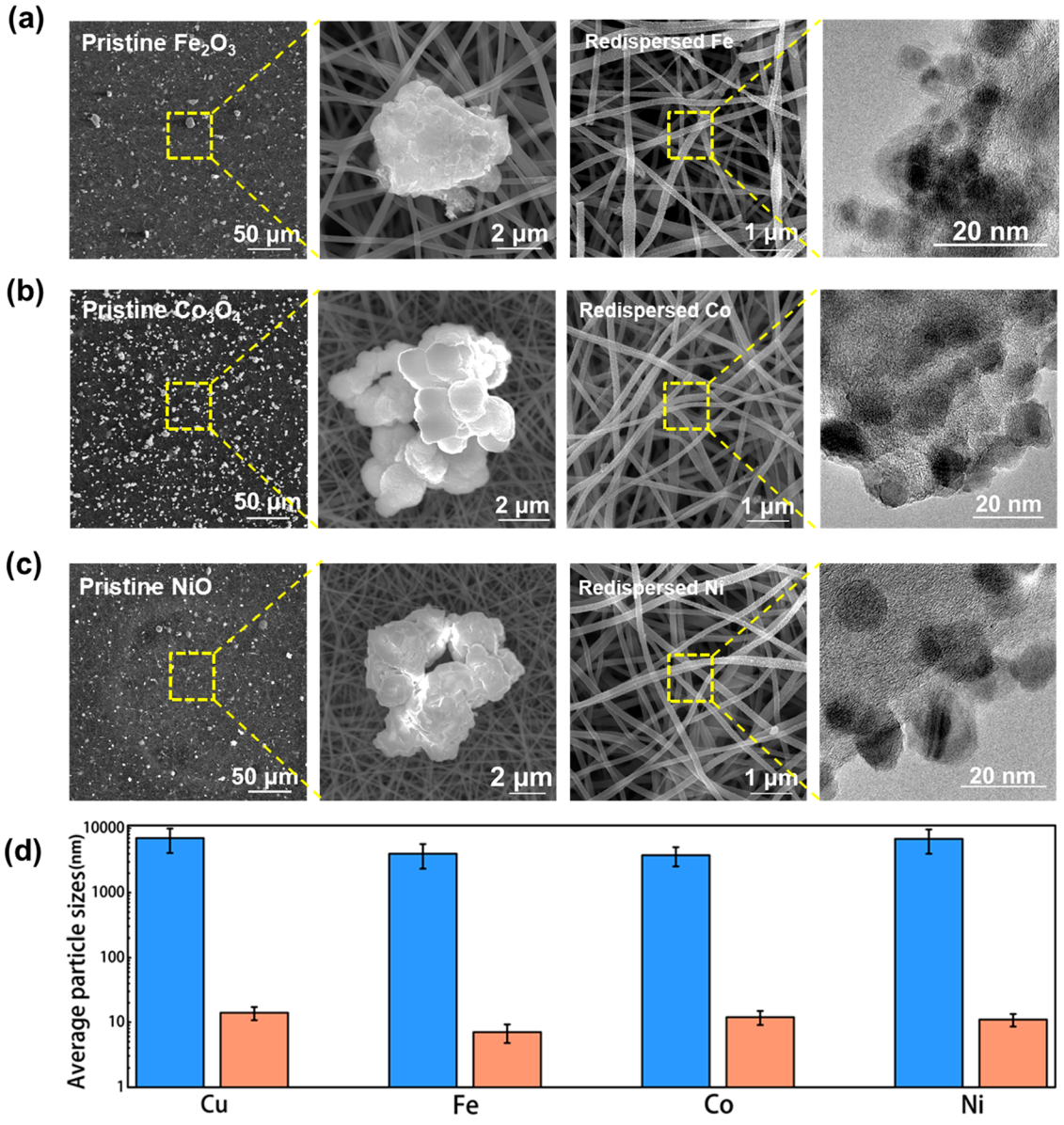

Figure 4. Universality of the high-temperature pulse method for various metal oxide and metal nanoparticles before and after redispersion, respectively, including (a) Fe_2O_3 and Fe, (b) Co_3O_4 and Co, and (c) NiO and Ni. (d) Statistics of the particle size change before (blue) and after (red) treatment.

The pulse temperature has a pronounced effect on the dispersing dimensions of the resulting nanoparticles. To study the impact of the heating temperature, we conducted the redispersion process using various heating currents and further characterized the samples by TEM. The current duration was carefully controlled at 100 ms, which is long enough to achieve a stable high-temperature plateau. We measured the temperature evolution profile of the CNF films, which we controlled by tuning the power source to achieve average plateau temperatures of 1380, 1600, 1800, and 1950 K [parts (a), (b), (c), and (d), respectively, of Figure 3). Parts (e), (f), (g), and (h) of Figure 3 show the general temperature distribution of the CNF films at these four different temperatures, respectively. The morphologies of the Cu nanoparticles after these different pulsed temperature treatments are shown in Figure 3i–l along with the corresponding size distributions, revealing an obvious temperature dependence.

Figure 3m illustrates the relationship between the pulse temperature and average particle size. Increasing the peak temperature from 1380 to 1800 K increases the dispersion effect as the average Cu nanoparticle size decreases. At ∼1800 K the nanoparticles reached a minimum average particle size compared to the other temperatures studied. We attribute this to the high mobility and migration capability of the metal atoms along the substrate surface induced by the high transient temperature. However, because of the competition between the atom movement and recoalescence, an increase in temperature to 1950 K resulted in a slight enlargement in the nanoparticle sizes. We hypothesize that the local bonding between the metal atoms and substrate cannot restrain atoms with high kinetic energy at higher temperature. Even though the average particle size at 1950 K is similar to that at 1380 K, the overall distribution morphology is not the same. Under the 1950 K condition, more of the nanoparticles are aggregated and sintered into larger ones, which we believe accounts for the

https://dx.doi.org/10.1021/jacs.0c04887
J. Am. Chem. Soc. 2020, 142, 17364−17371

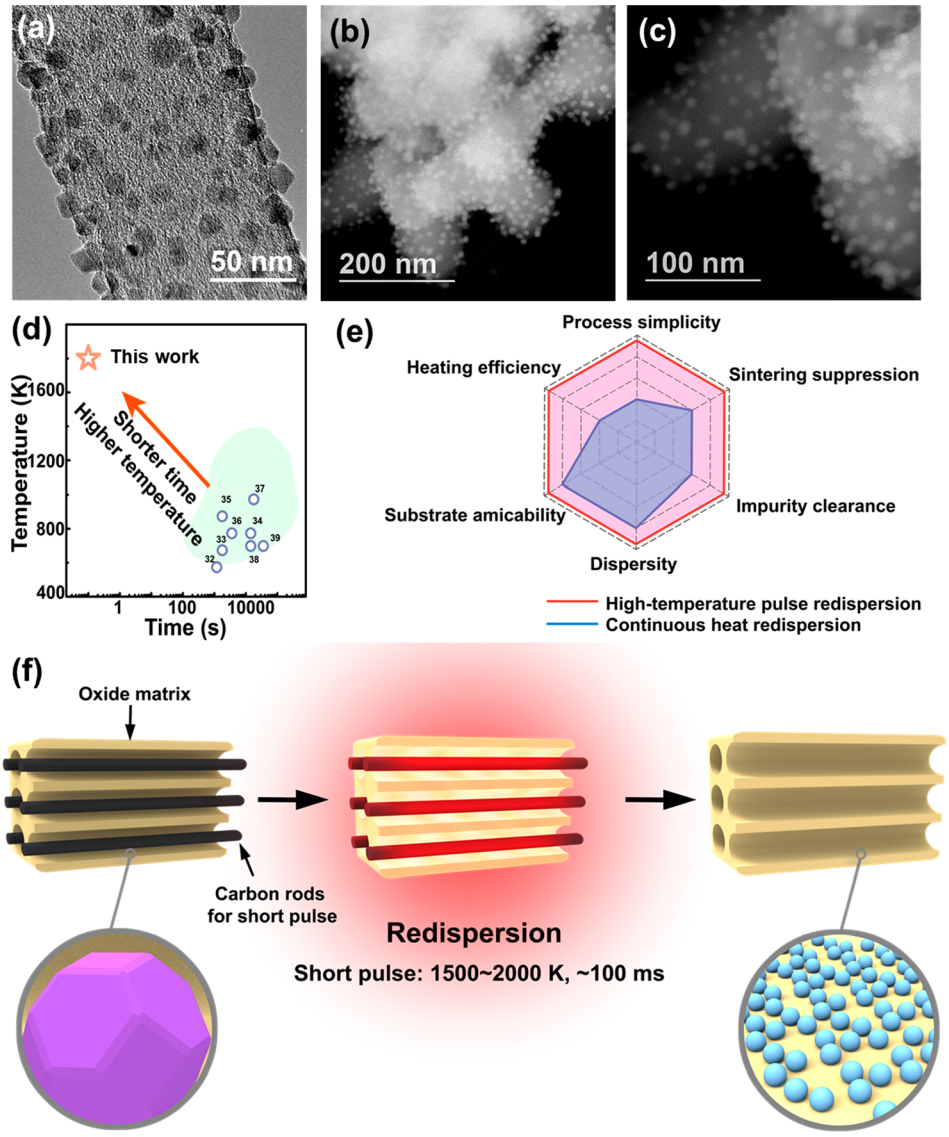

Figure 5. (a) TEM image of Cu nanoparticles redispersed from $CuCl_2$ particles. (b) and (c) STEM-HAADF images at different magnifications of Cu nanoparticles redispersed on a porous Al_2O_3 substrate. (d) Comparison of the heating time and temperature between this work and previous studies,[32−39] demonstrating the significantly shorter reaction time and higher heating temperature of our technique. (e) A radar plot showing a comparison between high-temperature pulse and continuous heat approaches to nanoparticle redispersion. (f) Schematic for the fast redispersion process of supported nanoparticle catalysts.

disappearance of ultrasmall particles. Similarly, the average distance between nanoparticles after the redispersion treatment at 1950 K is larger than that at 1380 K. Figure 3n provides a schematic of the fast redispersion process in which the oxide particles were broken down and redispersed/reduced as smaller nanoparticles.

Our redispersion method also demonstrates good universality in terms of materials. Figure 4a−c displays the morphology evolution of iron oxide (Fe_2O_3), cobalt oxide (Co_3O_4), and nickel oxide (NiO) particles before and after redispersion treatment at 1800 K for 100 ms. Though these starting metal oxide particles feature relatively large sizes from 0.1 to 10 μm, they still can be successfully dispersed by the high-temperature pulse treatment. The XRD patterns of these nanoparticles after treatment further confirmed their phase transition from oxidation states to metallic states (Figure S3). Note that all the three metals present face-centered cubic (fcc-Cu) structure owing to the quenching effect at a high-speed cooling rate. To better illustrate the redispersion capability for different particles, we plotted the size changes of the particles before and after redispersion (Figure 4d). The average particle sizes have decreased from several micrometers to ∼15 nm, which further confirmed the effectiveness of this high-temperature pulse method.

The high-temperature pulse technique can also help to eliminate some impurity elements. As chlorine poisoning can lead to the deactivation of nanoparticles for many reactions, its removal is critical to regain the active sites. Under the extreme heat generated by the high-temperature pulse technique, the chlorine can be effectively driven out of the nanoparticle. Figure 5a shows a TEM image of Cu nanoparticles redispersed from $CuCl_2$ particles in which the chlorine atoms are successfully eliminated with the help of the high-temperature treatment (Figure S4). This approach can also be applied on oxide substrates with good stability at high temperature for a short time, such as α-Al_2O_3. Figure 5b,c presents the scanning

https://dx.doi.org/10.1021/jacs.0c04887
J. Am. Chem. Soc. 2020, 142, 17364−17371

transmission electron microscopy high-angle annular dark-field (STEM-HAADF) images at different magnifications of Cu nanoparticles redispersed on porous α-Al_2O_3 substrates via the high-temperature pulse method. Because of the higher atomic number (Z) of copper, the nanoparticles appear brighter in contrast to the Al_2O_3 particle substrate in the HAADF mode. The Cu particle sizes can be effectively dispersed to under 10 nm with excellent uniformity via the high-temperature pulse at the temperature 1800 K for 100 ms. Redispersion on various substrates is presented in Figures S5−S8, including Ketjen-black carbon, reduced graphene oxide, and mesoporous silica. The dispersity of the nanoparticles demonstrates a pronounced dependence on the substrate, suggesting the need to tailor the high-temperature pulse treatment conditions.

Figure 5d presents a comparison of our work with results of previous particle redispersion studies.[32−39] Among these studies, our approach possesses the highest temperature and the shortest heating duration, making it a unique ultrafast redispersion process. A detailed procedure comparison is shown in Figures S9, S10, and Table S1. Figure 5e compares some key features of our high-temperature pulse treatment with standard continuous heating treatment utilizing a tube furnace. Compared to the standard continuous heating treatment, our approach shows advantages in processing simplicity, sintering suppression, and heat efficiency, which has the potential for fast redispersion applications. Figure 5f shows a schematic envisioning the direct redispersion engineering for commercial supported nanoparticle catalysts without further sophisticated particle−substrate separation. Carbon rods penetrate through the hollow voids of the substrates, on which the nanoparticle catalysts are degraded after long-term operation and the high-temperature pulse approach can effectively regenerate the nanoparticles on the porous substrates.

CONCLUSION

In conclusion, we report a facile redispersion technique for nanoparticles. We employed a CNF film as a heater and the treatment temperature was elevated to ∼1500−2000 K to enhance redispersion. The heating duration was kept to ∼100 ms, followed by a fast quenching process at a cooling rate of 10^5 K/s. Microscale particles were redispersed to the nanoscale and retained good uniformity. The amorphous carbon nanofiber film helped remove impurity elements during high-temperature pulse such as oxygen from the particles, regenerating them to their metallic state. Temperature profiles of the process can be tailored to vary the size and distribution of nanoparticles. For copper nanoparticles, the redispersion average sizes present a first decrease and then increase trend when the pulse temperature plateau varies from 1380 to 1950 K. Furthermore, the high-temperature pulse process is extremely rapid, which helps inhibit reagglomeration of the nanoparticles. Compared to current redispersion techniques based on continuous heating, our approach demonstrates the highest treatment temperature and shortest heating duration, which makes it a unique, ultrafast redispersion process. Our pulse redispersion technique also presents a universal and effective strategy for the redispersion of nanoparticle materials on different substrates and for a variety of applications.

METHODS

Preparation of CNF Films. An 8% by mass solution of polyacrylonitrile (PAN) (Sigma-Aldrich) in dimethylformamide (DMF) was electrospun at a voltage of 10 kV, a spinning distance of 15 cm, and a feeding rate of 1 mL/h. The as-spun nanofibers were collected by a rotation drum at a speed of 80 rpm. The electrospun film was then converted into CNFs by stabilizing in air at 280 °C for 5 h and carbonizing at 580 °C in an argon atmosphere.

Redispersion of Metal Nanoparticles. To make a CNF high-temperature heater, we connected a piece of CNF film with dimensions of 10 mm × 30 mm × 50 μm to copper electrodes and used silver paste to glue the film to the electrodes. The CNF film also functioned as the substrate for the nanoparticle redispersion. All metal oxides powders were purchased from Sigma-Aldrich: copper(II) oxide, iron(III) oxide, cobalt(II,III) oxide, and nickel(II) oxide. Metal oxides were weighed to 10 mg to mix with 10 mL of ethanol and sonicated for ∼1 h. A 10 μL suspension was transferred with a pipet and dropped on the substrates. For alumina and other substrates, oxide powders were mechanically mixed with substrates and grinded with mortar. The mixed powder was spread uniformly on the surface of the CNF heater. A current pulse was applied to the heater in an argon-filled glovebox using an external Keithley 2425 Source Meter to generate Joule heating. A Keithley 2400 source meter was employed to control the heating time. The source meter was connected to a Volteq HY 6020EX power supply to ensure power output. The applied voltage ranged from 0 to 60 V and the current ranged from 0 to 20 A.

Characterization. ImageJ software was employed to measure the nanoparticle diameters. For the particles before redispersion in Figure 4, the number of particles analyzed was ∼60. For the nanoparticles after redispersion, the number of particles analyzed was ∼100.

Inductively coupled plasma mass spectrometry was carried out with a PerkinElmer NexION 300D ICP Mass Spectrometer with autosampler.

The low-magnification morphological images of the particles were acquired using a field-emission SEM (Tescan XEIA FEG SEM). JEOL 2100F TEM at an accelerating voltage of 200 kV was used to characterize the nanoparticle morphologies at high resolution. The XRD patterns were achieved using a D8 Bruker Advanced X-ray Diffraction system.

Temperature Measurement. The temperature of the CNF was estimated according to the color ratio pyrometry by using a Vision Research Phantom Miro M110 high-speed camera with heating video recorded at 1000 frames/s. Some important variables are the channel gain (ψ_i), emissivity (ε), and spectral response (χ_i) of the camera at individual wavelengths and channels.[40] The gray-body assumption has been applied, substituted into Planck's Law, and integrated over the entire spectrum to which the camera is sensitive for the temperature estimation (as shown in eq 1 below). The normalized spectral response of the camera for the channel was reported by the manufacturer. By calibrating with a Newport Oriel 67000 Series Blackbody Infrared Light Source, we determined calibration factors C_{gr} (green/red), C_{bg} (blue/green), and C_{br} (blue/red) in eq 2 and presented them in Jacob and Kline et al. (assumed valid from 773 to 4773 K).[41]

$$\frac{I_i}{I_j} = \frac{\psi_i \int L(\varepsilon,\lambda,T)\,\chi_i(\lambda)\,\mathrm{d}\lambda}{\psi_j \int L(\varepsilon,\lambda,T)\,\chi_j(\lambda)\,\mathrm{d}\lambda} \tag{1}$$

$$\left(\frac{I_i}{I_j}\right) = C_{ij}\left(\frac{I_i}{I_j}\right)_{\varnothing} \tag{2}$$

MATLAB was used to extract raw pixel values and calculate temperatures. The demosaicing routine in MATLAB was used with the camera's Bayer color filter array to recover values for red, green, and blue channels at each pixel. To estimate the temperature, we used three color ratios (green/red, blue/green, and blue/red) simultaneously with minimized summed error and summed temperature errors greater than ∼110 K were eliminated. For the temperature profile, only unsaturated pixels above the black level and within the error threshold were used to report the mean and median temperature of the frame for a contiguous area of at least 10 acceptable pixels.

https://dx.doi.org/10.1021/jacs.0c04887
J. Am. Chem. Soc. 2020, 142, 17364−17371

Electrochemical Measurements. To briefly evaluate the catalytic activity of the redispersed nanoparticles, we carried out oxygen reduction linear sweep voltammetry for Pt particles on CNFs with and without redispersion using a rotating disk electrode (Figure 1b, Figure S1). Both Pt/CNF catalysts were mixed in aqueous solvent containing 0.05% Nafion and 10% isopropanol with a concentration of 1 mg/mL. The mixture was ultrasonicated for at least 30 min to achieve a homogeneous ink. The ink was then drop-casted onto a glassy carbon rotating disk electrode and allowed to dry to form a uniform catalyst film. Electrochemical tests were conducted with a Pine Research rotation disk electrode test system. Ag/AgCl and graphite rod were adopted as the reference and counter electrodes, respectively. Fifty milliliters of 1 M KOH was prepared with deionized water and implemented as the electrolyte. Polarization curves were measured at a rotation speed of 1600 rpm.

■ ASSOCIATED CONTENT

Supporting Information

The Supporting Information is available free of charge at https://pubs.acs.org/doi/10.1021/jacs.0c04887.

Oxygen reduction activity of the Pt particles, Raman spectra of the substrate XRD patterns of the redispersed nanoparticles, redispersion of nanoparticles on various substrates, and a comparison between redispersion methods (PDF)

■ AUTHOR INFORMATION

Corresponding Author

Liangbing Hu − *Department of Materials Science and Engineering, University of Maryland, College Park, Maryland 20742, United States;* orcid.org/0000-0002-9456-9315; Email: binghu@umd.edu

Authors

Hua Xie − *Department of Materials Science and Engineering, University of Maryland, College Park, Maryland 20742, United States*

Min Hong − *Department of Materials Science and Engineering, University of Maryland, College Park, Maryland 20742, United States*

Emily M. Hitz − *Department of Materials Science and Engineering, University of Maryland, College Park, Maryland 20742, United States*

Xizheng Wang − *Department of Materials Science and Engineering, University of Maryland, College Park, Maryland 20742, United States*

Mingjin Cui − *Department of Materials Science and Engineering, University of Maryland, College Park, Maryland 20742, United States*

Dylan J. Kline − *Department of Environmental and Chemical Engineering, University of California Riverside, Riverside, California 92521, United States;* orcid.org/0000-0001-8800-2841

Michael R. Zachariah − *Department of Environmental and Chemical Engineering, University of California Riverside, Riverside, California 92521, United States;* orcid.org/0000-0002-4115-3324

Complete contact information is available at: https://pubs.acs.org/10.1021/jacs.0c04887

Author Contributions

#H.X. and M.H. contributed equally to this work.

Notes

The authors declare no competing financial interest.

■ ACKNOWLEDGMENTS

We acknowledge the support of the Maryland Nanocenter, its Surface Analysis Center, and AIMLab.

■ REFERENCES

(1) Meng, C.; Muralidharan, N.; Teblum, E.; Moyer, K. E.; Nessim, G. D.; Pint, C. L. Multifunctional Structural Ultrabattery Composite. *Nano Lett.* **2018**, *18* (12), 7761−7768.

(2) Liu, W.; Li, H.; Jin, J.; Wang, Y.; Zhang, Z.; Chen, Z.; Wang, Q.; Chen, Y.; Paek, E.; Mitlin, D. Synergy of Epoxy Chemical Tethers and Defect-Free Graphene in Enabling Stable Lithium Cycling of Silicon Nanoparticles. *Angew. Chem.* **2019**, *131* (46), 16743−16753.

(3) Lacey, S. D.; Dong, Q.; Huang, Z.; Luo, J.; Xie, H.; Lin, Z.; Kirsch, D. J.; Vattipalli, V.; Povinelli, C.; Fan, W.; Shahbazian-Yassar, R.; Wang, D.; Hu, L. Stable Multimetallic Nanoparticles for Oxygen Electrocatalysis. *Nano Lett.* **2019**, *19* (8), 5149−5158.

(4) Liu, M.; Zhang, Z.; Okejiri, F.; Yang, S.; Zhou, S.; Dai, S. Entropy-Maximized Synthesis of Multimetallic Nanoparticle Catalysts via a Ultrasonication-Assisted Wet Chemistry Method under Ambient Conditions. *Adv. Mater. Interfaces* **2019**, *6* (7), 1900015.

(5) Li, Y.; Sun, Y.; Qin, Y.; Zhang, W.; Wang, L.; Luo, M.; Yang, H.; Guo, S. Recent Advances on Water-Splitting Electrocatalysis Mediated by Noble-Metal-Based Nanostructured Materials. *Adv. Energy Mater.* **2020**, *10* (11), 1903120.

(6) Morgan, K.; Goguet, A.; Hardacre, C. Metal Redispersion Strategies for Recycling of Supported Metal Catalysts: A Perspective. *ACS Catal.* **2015**, *5* (6), 3430−3445.

(7) Nagai, Y.; Dohmae, K.; Ikeda, Y.; Takagi, N.; Tanabe, T.; Hara, N.; Guilera, G.; Pascarelli, S.; Newton, M. A.; Kuno, O.; Jiang, H.; Shinjoh, H.; Matsumoto, S. In Situ Redispersion of Platinum Autoexhaust Catalysts: An on-Line Approach to Increasing Catalyst Lifetimes? *Angew. Chem., Int. Ed.* **2008**, *47* (48), 9303−9306.

(8) Alonso, F.; Riente, P.; Sirvent, J. A.; Yus, M. Nickel Nanoparticles in Hydrogen-Transfer Reductions: Characterisation and Nature of the Catalyst. *Appl. Catal., A* **2010**, *378* (1), 42−51.

(9) Rusevova, K.; Kopinke, F. D.; Georgi, A. Nano-Sized Magnetic Iron Oxides as Catalysts for Heterogeneous Fenton-like Reactions-Influence of Fe(II)/Fe(III) Ratio on Catalytic Performance. *J. Hazard. Mater.* **2012**, *241*−*242*, 433−440.

(10) Du, L.; Shao, Y.; Sun, J.; Yin, G.; Liu, J.; Wang, Y. Advanced Catalyst Supports for PEM Fuel Cell Cathodes. *Nano Energy* **2016**, *29*, 314−322.

(11) Tuxen, A.; Carenco, S.; Chintapalli, M.; Chuang, C. H.; Escudero, C.; Pach, E.; Jiang, P.; Borondics, F.; Beberwyck, B.; Alivisatos, A. P.; Thornton, G.; Pong, W. F.; Guo, J.; Perez, R.; Besenbacher, F.; Salmeron, M. Size-Dependent Dissociation of Carbon Monoxide on Cobalt Nanoparticles. *J. Am. Chem. Soc.* **2013**, *135* (6), 2273−2278.

(12) Bergamaski, K.; Pinheiro, A. L. N.; Teixeira-Neto, E.; Nart, F. C. Nanoparticle Size Effects on Methanol Electrochemical Oxidation on Carbon Supported Platinum Catalysts. *J. Phys. Chem. B* **2006**, *110* (39), 19271−19279.

(13) Iablokov, V.; Beaumont, S. K.; Alayoglu, S.; Pushkarev, V. V.; Specht, C.; Gao, J.; Alivisatos, A. P.; Kruse, N.; Somorjai, G. A. Size-Controlled Model Co Nanoparticle Catalysts for CO 2 Hydrogenation: Synthesis, Characterization, and Catalytic Reactions. *Nano Lett.* **2012**, *12* (6), 3091−3096.

(14) Saha, J.; Bhowmik, K.; Das, I.; De, G. Pd-Ni Alloy Nanoparticle Doped Mesoporous SiO2 Film: The Sacrificial Role of Ni to Resist Pd-Oxidation in the C-C Coupling Reaction. *Dalt. Trans.* **2014**, *43* (35), 13325−13332.

(15) Desforges, A.; Backov, R.; Deleuze, H.; Mondain-Monval, O. Generation of Palladium Nanoparticles within Macrocellular Polymeric Supports: Application to Heterogeneous Catalysis of the

Suzuki-Miyaura Coupling Reaction. *Adv. Funct. Mater.* **2005**, *15* (10), 1689−1695.
(16) Diallo, A. K.; Ornelas, C.; Salmon, L.; Ruiz Aranzaes, J.; Astruc, D. Homeopathic" Catalytic Activity and Atom-Leaching Mechanism in Miyaura-Suzuki Reactions under Ambient Conditions with Precise Dendrimer-Stabilized Pd Nanoparticles. *Angew. Chem., Int. Ed.* **2007**, *46* (45), 8644−8648.
(17) Niu, Z.; Peng, Q.; Zhuang, Z.; He, W.; Li, Y. Evidence of an Oxidative-Addition-Promoted Pd-Leaching Mechanism in the Suzuki Reaction by Using a Pd-Nanostructure Design. *Chem. - Eur. J.* **2012**, *18* (32), 9813−9817.
(18) Broqvist, P.; Molina, L. M.; Grönbeck, H.; Hammer, B. Promoting and Poisoning Effects of Na and Cl Coadsorption on CO Oxidation over MgO-Supported Au Nanoparticles. *J. Catal.* **2004**, *227* (1), 217−226.
(19) Ellis, P. J.; Fairlamb, I. J. S.; Hackett, S. F. J.; Wilson, K.; Lee, A. F. Evidence for the Surface-Catalyzed Suzuki-Miyaura Reaction over Palladium Nanoparticles: An Operando XAS Study. *Angew. Chem., Int. Ed.* **2010**, *49* (10), 1820−1824.
(20) Sá, J.; Goguet, A.; Taylor, S. F. R.; Tiruvalam, R.; Kiely, C. J.; Nachtegaal, M.; Hutchings, G. J.; Hardacre, C. Influence of Methyl Halide Treatment on Gold Nanoparticles Supported on Activated Carbon. *Angew. Chem., Int. Ed.* **2011**, *50* (38), 8912−8916.
(21) Heck, K. N.; Nutt, M. O.; Alvarez, P.; Wong, M. S. Deactivation Resistance of Pd/Au Nanoparticle Catalysts for Water-Phase Hydrodechlorination. *J. Catal.* **2009**, *267* (2), 97−104.
(22) Ruckenstein, E.; Chu, Y. F. Redispersion of Platinum Crystallites Supported on Alumina-Role of Wetting. *J. Catal.* **1979**, *59* (1), 109−122.
(23) Campbell, C. T. The Energetics of Supported Metal Nanoparticles: Relationships to Sintering Rates and Catalytic Activity. *Acc. Chem. Res.* **2013**, *46* (8), 1712−1719.
(24) Rice, R. W.; Chien, C. C. Simulation of Supported Iridium Catalyst Sintering and Redispersion. *J. Catal.* **1987**, *103* (1), 140−150.
(25) Tatarchuk, B. J.; Dumesic, J. A. Physical Characterization of Fe/TiO2Model Supported Catalysts. *J. Catal.* **1981**, *70*, 308−322.
(26) Glassl, H.; Hayek, K.; Kramer, R. Electron Microscopy of Pt/Al2O3Model Catalysts. *J. Catal.* **1981**, *68*, 397−405.
(27) Hoch, L. B.; Mack, E. J.; Hydutsky, B. W.; Hershman, J. M.; Skluzacek, J. M.; Mallouk, T. E. Carbothermal Synthesis of Carbon-Supported Nanoscale Zero-Valent Iron Particles for the Remediation of Hexavalent Chromium. *Environ. Sci. Technol.* **2008**, *42* (7), 2600−2605.
(28) Guo, X.; Hao, C.; Jin, G.; Zhu, H. Y.; Guo, X. Y. Copper Nanoparticles on Graphene Support: An Efficient Photocatalyst for Coupling of Nitroaromatics in Visible Light. *Angew. Chem., Int. Ed.* **2014**, *53* (7), 1973−1977.
(29) Li, H. H.; Cui, C. H.; Zhao, S.; Yao, H.-B.; Gao, M. R.; Fan, F. J.; Yu, S. H. Mixed-Ptpd-Shell Ptpdcu Nanoparticle Nanotubes Templated from Copper Nanowires as Effi Cient and Highly Durable Electrocatalysts. *Adv. Energy Mater.* **2012**, *2* (10), 1182−1187.
(30) Prieto, G.; Zečević, J.; Friedrich, H.; De Jong, K. P.; De Jongh, P. E. Towards Stable Catalysts by Controlling Collective Properties of Supported Metal Nanoparticles. *Nat. Mater.* **2013**, *12* (1), 34.
(31) O'Neill, B. J.; Jackson, D. H. K.; Crisci, A. J.; Farberow, C. A.; Shi, F.; Alba-Rubio, A. C.; Lu, J.; Dietrich, P. J.; Gu, X.; Marshall, C. L.; Stair, P. C.; Elam, J. W.; Miller, J. T.; Ribeiro, F. H.; Voyles, P. M.; Greeley, J.; Mavrikakis, M.; Scott, S. L.; Kuech, T. F.; Dumesic, J. A. Stabilization of Copper Catalysts for Liquid-Phase Reactions by Atomic Layer Deposition. *Angew. Chem., Int. Ed.* **2013**, *52* (51), 13808−13812.
(32) Kartusch, C.; Krumeich, F.; Safonova, O.; Hartfelder, U.; Makosch, M.; Sá, J.; Van Bokhoven, J. A. Redispersion of Gold Multiple-Twinned Particles during Liquid-Phase Hydrogenation. *ACS Catal.* **2012**, *2* (7), 1394−1403.
(33) Nagai, Y.; Hirabayashi, T.; Dohmae, K.; Takagi, N.; Minami, T.; Shinjoh, H.; Matsumoto, S. Sintering Inhibition Mechanism of Platinum Supported on Ceria-Based Oxide and Pt-Oxide-Support Interaction. *J. Catal.* **2006**, *242* (1), 103−109.
(34) Okal, J.; Kępiński, L.; Krajczyk, L.; Drozd, M. Oxidation and Redispersion of a Re/γ-Al2O3 Catalyst. *J. Catal.* **1999**, *188* (1), 140−153.
(35) Wu, T.; Pan, X.; Zhang, Y.; Miao, Z.; Zhang, B.; Li, J.; Yang, X. Investigation of the Redispersion of Pt Nanoparticles on Polyhedral Ceria Nanoparticles. *J. Phys. Chem. Lett.* **2014**, *5* (14), 2479−2483.
(36) Arteaga, G. J.; Anderson, J. A.; Rochester, C. H. Effects of Oxidation-Reduction and Oxychlorination-Reduction Cycles on CO Adsorption by Pt-Sn/Al2O3 Catalysts. *J. Catal.* **1999**, *184* (1), 268−279.
(37) Tanabe, T.; Nagai, Y.; Dohmae, K.; Sobukawa, H.; Shinjoh, H. Sintering and Redispersion Behavior of Pt on Pt/MgO. *J. Catal.* **2008**, *257* (1), 117−124.
(38) Weststrate, C. J.; Hauman, M. M.; Moodley, D. J.; Saib, A. M.; Van Steen, E.; Niemantsverdriet, J. W. Cobalt Fischer−Tropsch Catalyst Regeneration: The Crucial Role of the Kirkendall Effect for Cobalt Redispersion. *Top. Catal.* **2011**, *54* (13−15), 811−816.
(39) Hauman, M. M.; Saib, A.; Moodley, D. J.; duPlessis, E.; Claeys, M.; VanSteen, E. Re-Dispersion of Cobalt on a Model Fischer−Tropsch Catalyst During Reduction-Oxidation-Reduction Cycles. *ChemCatChem* **2012**, *4* (9), 1411−1419.
(40) Fu, T.; Wang, Z.; Cheng, X. Temperature Measurements of Diesel Fuel Combustion with Multicolor Pyrometry. *J. Heat Transfer* **2010**, *132* (5), 1−7.
(41) Jacob, R. J.; Kline, D. J.; Zachariah, M. R. High Speed 2-Dimensional Temperature Measurements of Nanothermite Composites: Probing Thermal vs. Gas Generation Effects. *J. Appl. Phys.* **2018**, *123* (11), 115902.

https://dx.doi.org/10.1021/jacs.0c04887
J. Am. Chem. Soc. 2020, 142, 17364−17371